Relaxation Nuclear Magnetic Resonance Imaging Investigation of Heterogeneous Aging in a Hydroxy-Terminated Polybutadiene-Based Elastomer

T. M. Alam,*,† B. R. Cherry,†,§ K. R. Minard,‡ and M. Celina†

Sandia National Laboratories, Albuquerque, New Mexico 87185, and Pacific Northwest National Laboratory, Richland, Washington 99352

Received August 31, 2005; Revised Manuscript Received October 6, 2005

ABSTRACT: Relaxation nuclear magnetic resonance imaging (R-NMRI) was employed to investigate the effects of thermooxidative aging in a hydroxy-terminated polybutadiene (HTPB)-based elastomer. A series of three-dimensional (3D) Hahn-echo-weighted single-point images (SPI) of the elastomer were utilized to generate a 3D parameter map of the aged material. NMR spin−spin relaxation times (T_2) were measured for each voxel producing a 3D NMR parameter (T_2) map of the aged polymer. These T_2 maps reveal a dramatic reduction of local polymer mobility near the aging surface with the degree of T_2 heterogeneity varying as a function of aging. Using correlations between NMR T_2 and material modulus, the impact of this heterogeneous thermooxidative aging on the material properties is discussed.

Introduction

Polybutadiene-based elastomers are widely used as binders in solid propellant grain. Understanding their long-term aging characteristics is critical for performance assessment and lifetime prediction of such materials.[1] In particular, the thermooxidative aging of a hydroxy-terminated polybutadiene (HTPB) crosslinked with isophorone diisocyanate (IPDI) has been investigated extensively.[1−3] Using sensitive oxidation rate measurements, it was shown that oxidative degradation is a determining factor in aging related changes of mechanical properties (loss in tensile elongation and modulus increases) and is associated with further crosslinking, densification, and reduced polymer mobility.[3] NMR spectroscopy is an appealing technique to probe for molecular mobility via relaxation times. NMR parameters have been correlated with other material changes and have been used for condition monitoring of the polymer.[3−6] Recently a critical comparison of the sensitivity of proton relaxation times as a function of temperature was conducted.[7] One of the important issues to consider for accelerated thermooxidative aging of elastomers is the development of heterogeneities in the degradation process. Heterogeneities have been discussed as originating on the molecular level due to restricted mobilities of free radicals and preferential initiation reactions[8−10] and on a more macroscopic scale due to diffusion-limited oxidation (DLO) effects.[11−13] DLO conditions lead to pronounced spatial variations in elastomer hardening and related properties and have been successfully verified using micromodulus profiling techniques,[13,14] including experimental data for the current HTPB material.[3] The development of new experimental techniques that can probe this spatial heterogeneity or variation in aged polymers is therefore important.

Nuclear magnetic resonance imaging (NMRI)[15] or NMR microscopy (**k**-space imaging)[16] is an experimental technique that has seen an ever-increasing role in material science, particularly in the spatial analysis of polymers and composites.[17−22] A common difficulty encountered in NMRI of materials is that low molecular mobility and significant ^{1}H−^{1}H dipolar coupling result in very short ^{1}H NMR spin−spin T_2 relaxation times. Because of the time scale of common imaging pulse sequences, the short T_2 can strongly limit the performance of direct image methods within materials. A variety of experimental NMRI approaches have been developed to compensate for this shortcoming. For example, one common practice in imaging of polymers is to swell samples in a solvent.[23−34] It is then possible to obtain NMR images of the solvent, since these small molecules typically have rapid molecular motion and longer T_2 relaxation times. In many instances the uptake of solvent can also significantly increase the molecular level polymer motions, thereby increasing the observed T_2 relaxation rate of polymer nuclei, facilitating direct imaging of the solid polymer. A difficulty in utilizing solvents to swell polymers prior to NMR imaging is the complication of differential swelling or expansion due to heterogeneities within the polymer, leading to a corresponding distortion of the spatial image. Another approach that allows NMR imaging techniques to be utilized in materials is the incorporation of pulse sequences amenable to short T_2 values, avoiding the need for solvent swelling. These techniques include single-point imaging (SPI) and multipoint (MP) **k**-space mapping[35−41] and have permitted high-resolution images in a variety of solid materials to be obtained, including direct imaging of polymer samples.[23,42−49]

A benefit of using NMRI is the ability to couple traditional NMR spectroscopy techniques with imaging to provide a measurement of local nuclei spin behavior at a particular position (image voxel) in addition to measuring simple spin concentration or density. One common example is incorporating different NMR pulse sequences to provide image contrast or directly measure NMR spin relaxation parameters. These types of NMRI

† Sandia National Laboratories.
‡ Northwest National Laboratory.
§ Current address: Bruker Biospin Corp., Billerica, MA 01821.
* Corresponding author: Ph (505) 844-1225; Fax (505) 844-2974; e-mail tmalam@sandia.gov.

10.1021/ma051906y CCC: $30.25
Published on Web 11/19/2005

experiments include spin−spin (T_2), spin−lattice (T_1), and rotating frame spin ($T_{1\rho}$) relaxation-based experiments. The reader is referred to more comprehensive review articles and books on the subject of NMRI and relaxation filters.[21,50−53] In many instances the NMR relaxation parameters can be directly correlated to physical properties within the material. For example, the NMR ^{1}H T_2 relaxation time has been shown to be a sensitive measure of local chain mobility and is inversely proportional to the square of the reduced effective dipolar coupling.[54−56,57] Changes in the NMR T_2 relaxation times have been correlated to polymer modulus, induced stress, cross-link density, and/or the degree of polymer chain entanglement. By incorporating these types of NMR relaxation/physical property correlations, it is possible to create unique spatial property images within materials. Parameter-related images are also known as material property images (MAP images).[20] Examples of relaxation maps in polymers include $T_{1\rho}$ studies of cross-linking in natural rubbers and polybutadiene,[23,42−44] T_2 maps of cross-link density in rubber and polyisobutylene,[20,33] multiple quantum-filtered and T_2 maps of strained elastomers and tendons,[45,47,58] T_2 maps of solvent permeation,[33,49] aging and boundary migration in natural rubbers,[46,59] and T_1 and T_2 maps of anisotropic molding effects in high-density polyethylene (HDPE).[48]

The use of NMRI to investigate polymer aging and degradation has been more limited. Over a decade ago Blümer and Blümich reported the three-dimensional (3D) T_2 maps of natural rubber thermally aged in air, clearly revealing growth of surface hardening with aging time.[19] NMRI has also been used to investigate biodegradation of polymer films,[60] the aging in nitrile rubber elastometrs,[59] and the degradation of rubber and polystyrene.[61] In addition, two-dimensional (2D) $T_{1\rho}$ and T_2 maps have been obtained for oxidative aging of natural rubbers,[43,62] T_2 maps of silicone copolymers during long-term desiccation,[63] and 3D maps of radiation effects in polymer gels have also been reported.[64] In this paper, we describe the use of NMRI to produce 3D T_2 spatial maps of aging in a HTPB/IPDI polyurethane binder. Heterogeneous spatial variation in the NMR T_2 is observed due to diffusion-limited oxidation (DLO) as a function of distance from the polymer surface.

Experimental Section

The polybutadiene-based elastomer investigated was a cured hydroxy-terminated polybutadiene (HTPB)/isophorone diisocyanate (IPDI) copolymer. The uncured resins were provided by Elf Atochem and Hüls America Inc. The bulk characterization, thermal and oxidative aging, and modulus profiling for these binders have been previously described.[3,4] The sample used in this study was aged for 8 days at 125 °C under ambient atmospheric conditions (∼630 mmHg in Albuquerque, NM).

A 2.0 mm × 2.5 mm × 2.5 mm piece of the polyurethane material was cut from the aged polymer pad and placed in a home-built microimaging probe with a 5 mm diameter rf coil and a custom-built 8 mm diameter gradient coil. The images were collected with a Varian Inova wide-bore spectrometer operating at a ^{1}H Larmor frequency of 500 MHz. To handle the relatively short T_2 times present in the polymer binder, a 3D SPI experiment was coupled to a Hahn echo as described by Beyea and co-workers.[65] The imaging pulse sequence is shown in Figure 1. The Hahn-echo preparation period for T_2 measurement utilized echo delays (τ) of 0, 0.3, and 1 ms and an acquisition delay period (t_p) of 60 μs. The SPI experiment used a maximum gradient strength of 230 G/cm and 16 × 32 × 16 phase encoding gradient steps to obtain a 3D image

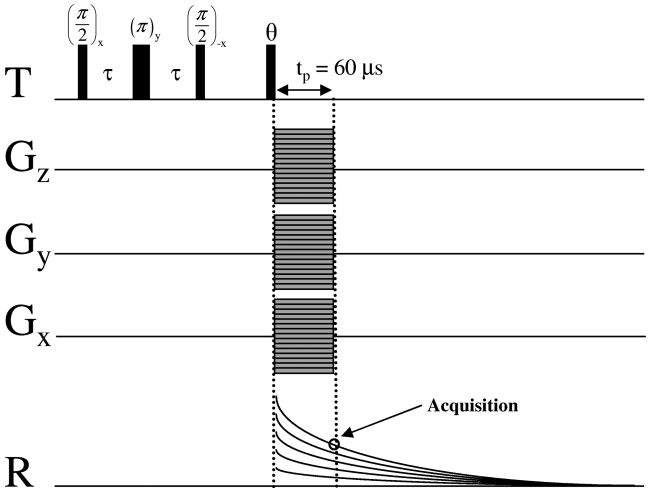

Figure 1. R-NMRI pulse sequence utilized. A Hahn echo was coupled to a 3D single-point imaging (SPI) pulse sequence through a 90° pulse which acts as a z-filter.[65] G_x, G_y, and G_z correspond to the gradient pulses applied along orthogonal directions, and T and R represent the transmitter rf pulse and receiver channels, respectively. The acquisition delay t_p was 60 μs for all experiments.

characterized by a field-of-view (FOV) of 2.5 mm (X) × 3.5 mm (Y) × 3.5 mm (Z) and a spatial resolution of 156 × 109 × 219 μm along each axis. Final images were then Fourier reconstructed using a 32 × 64 × 32 matrix containing 65 536 voxels. The voxel size is therefore half the actual spatial resolution encoded along each axis and corresponds to a volume element of 0.000 47 mm^3. Data collection for each 3D image was ∼18 h. Because of instrumental time limitations, images for only three different τ values were obtained. Bulk T_2 relaxation NMR experiments were also obtained for the unaged and aged binder samples. These bulk relaxation results are presented in the Supporting Information for the unaged (Figure 1S) and aged (Figure 2S) HTPB binder. These bulk T_2 experiments show a multi-exponential decay of the magnetization, with approximately 80−90% of the total signal intensity rapidly decaying (short T_2), followed by a minor component that has a longer T_2 time. For decay times between 60 μs (t_p) and 2 ms the signal intensity decay is describe very well by a single exponential (Figures 1S(b) and 2S(b) in Supporting Information). For the decay times selected in the NMR imaging experiment the signal intensity $I(\tau)$ for each voxel can therefore be described by a single-exponential decay with a T_2 relaxation time via

$$I(\tau) \sim \exp\left(\frac{-2\tau}{T_2}\right) \quad (1)$$

where τ is the echo delay time defined in Figure 1. The T_2 values for each voxel were calculated using MATLAB (MathWorks, Inc., Natick, MA) fitting a linear natural log representation of the single-exponential decay described by eq 1.

Results and Discussion

The 3D SPI ^{1}H NMR image of the aged polyurethane, obtained with no delay in the Hahn echo, is shown in Figure 2. The individual sectional planar slices (XY plane) are presented in Figure 2a and were used to obtain the complete reconstructed 3D NMR image (Figure 2c). The photo in Figure 2b demonstrates the relative size of the polymer sample investigated. The aged binder was oriented with the thermooxidatively aged surface nominally parallel to the XZ plane. In this arrangement, the aging and oxidation effects are greatest at polymer interface at the top and bottom of the individual 2D slices in Figure 2a. The 28 planar images

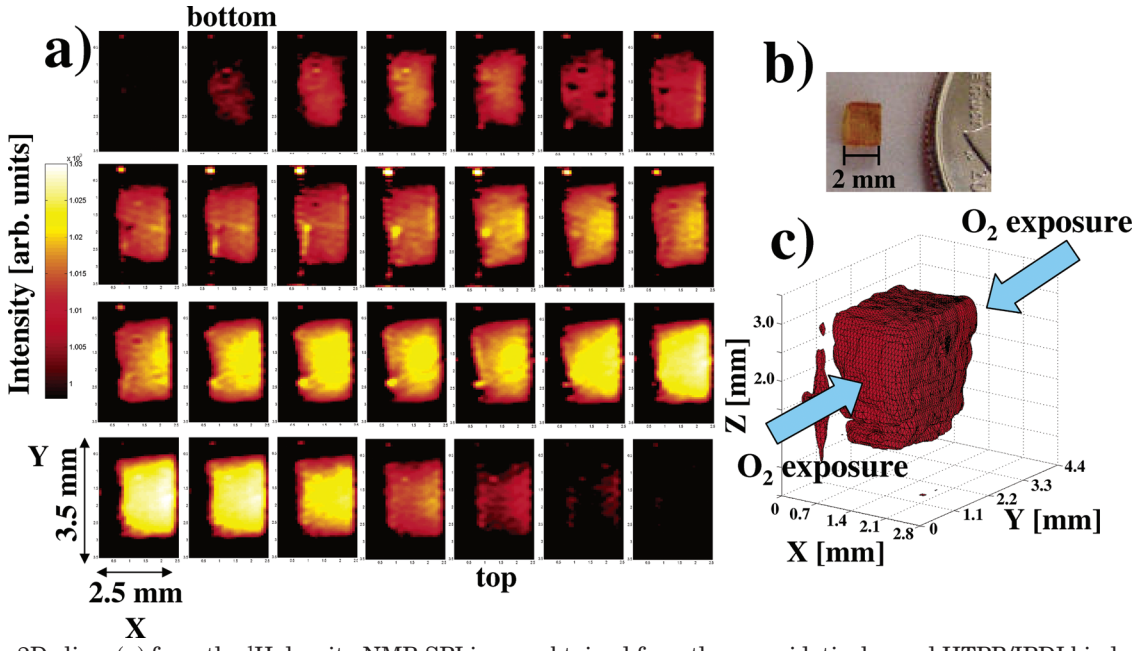

Figure 2. 2D slices (a) from the ^{1}H density NMR SPI image obtained for a thermooxidatively aged HTPB/IPDI binder. Each 2D image (110 μm thick) is an *XY* plane through the material with the aged surfaces at the top and bottom of the individual slices. The field of view for each slice is 2.5 mm × 3.5 mm and has a voxel resolution of 78 μm × 55 μm. Photograph of the aged polyurethane sample used (b). The reconstructed 3D SPI NMR image (c) of the binder sample, along with the definition of axes and the aging surfaces.

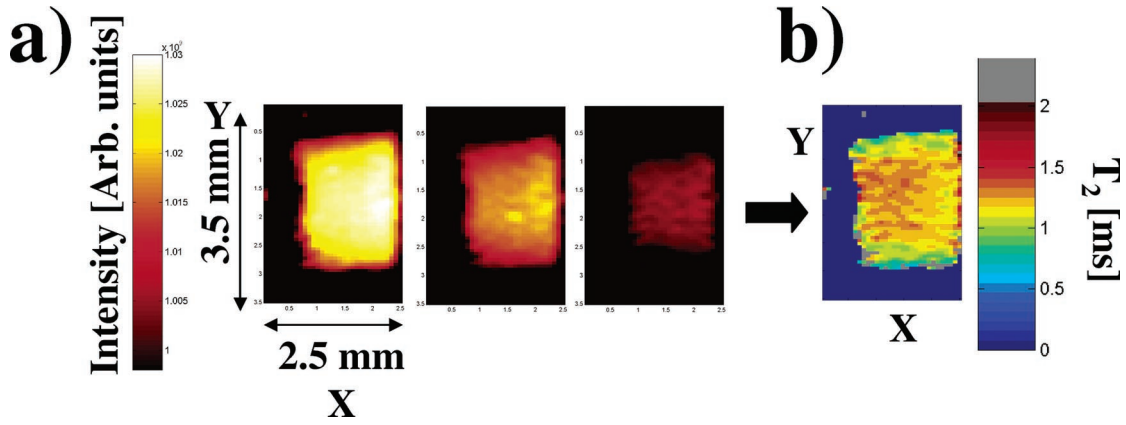

Figure 3. A series of 2D slices (a) taken of the same spatial region of the thermooxidatively aged HTPB/IPDI binder for three different Hahn-echo delays (τ). The resulting T_2 relaxation map (b) calculated from the decay of signal intensity for each voxel using eq 1, with the corresponding T_2 color bar on the right ranging from 0 to 2 ms.

are arranged such that the first 2D *XY* plane in the upper left of Figure 2a is the empty space below the sample, with the successive 2D slices moving through the sample of aged binder from bottom to top (moving from left to right and row by row though Figure 2a). The voxel dimensions are 78 × 55 × 110 μm, giving a 0.000 47 mm^3 volume for each imaging voxel element.

The 3D ^{1}H NMR image of the HTPB binder in Figure 2 does not reveal any distinct variations or spatial homogeneities within the sample as a result of thermal aging. This lack of variation in the ^{1}H spin density images is not surprising since aging is not expected to produce major changes in the local polymer concentration or density. There are voids in the binder sample observed as black regions in the NMRI slices (for example see the top row of images in Figure 2a). The typical dimension of the observed voids was on the order of ~200 μm × 200 μm × 200 μm (0.008 mm^3), but one void was observed to extended nearly 600 μm in one dimension. The presence of voids in cross-linked elastomers has been shown to be an indicator for crack initiation and mechanical failure.[26] In the present example the concentration of these voids is not high. Therefore, we do not expect these voids to greatly impact the aging of the material, so their presence was not considered important. It should be noted that there was a subtle variation in the T_2 relaxation time distribution for regions that contained pores as discussed below.

It has been demonstrated that polymer material NMR relaxation maps often reveal variations in the material physical properties that are not readily visible in the direct ^{1}H NMR spin density images.[19,21,43,59,63] In the present study ^{1}H T_2 relaxation maps were generated by obtaining additional 3D NMR SPI images (not shown) for different interpulse lengths (τ) of the Hahn-echo prefilter (Figure 1) to obtain a measure of the T_2 relaxation time using eq 1. An example of the procedure is shown in Figure 3a, where the effects of different Hahn-echo τ spacing on the individual voxel signal intensities for a representative 2D image slice (*XY* plane) are used to produce the T_2 relaxation map (Figure 3b).

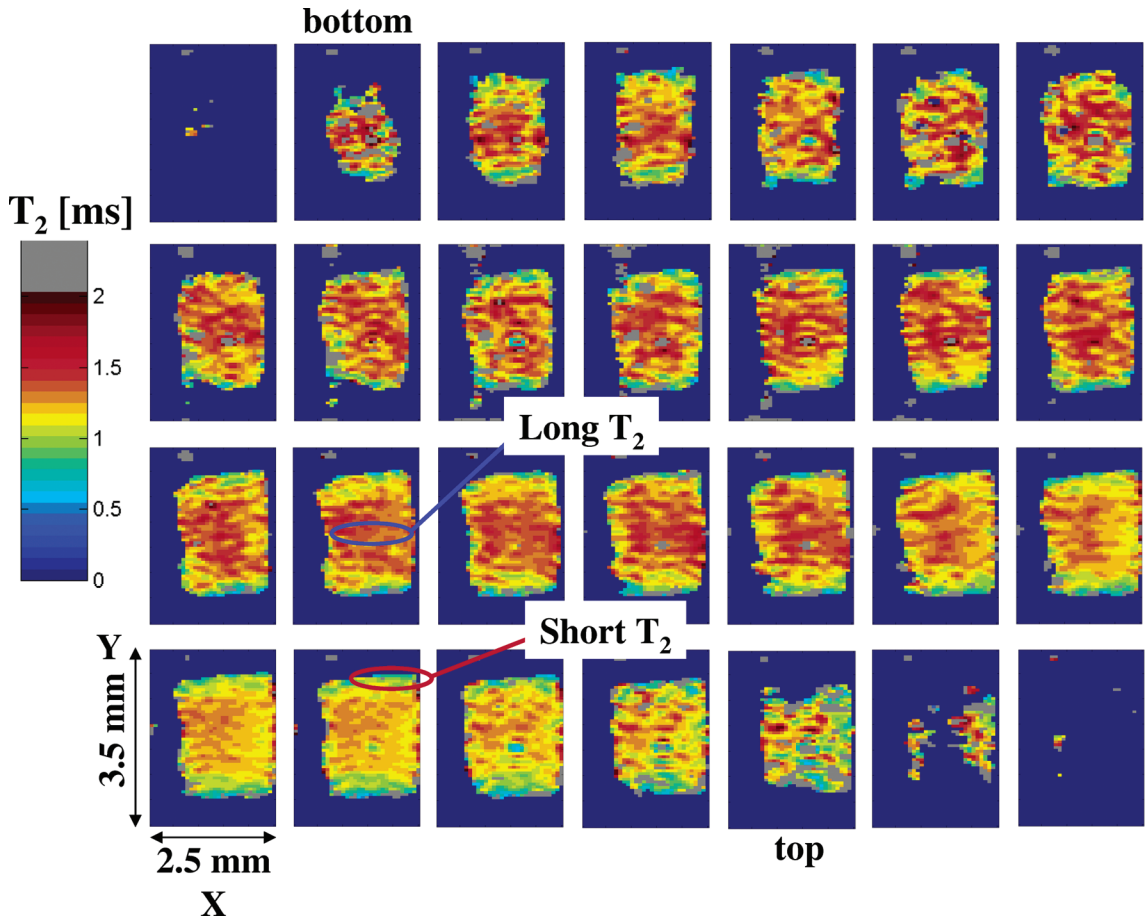

Figure 4. Three-dimensional NMR spin−spin relaxation time T_2 map of the thermooxidatively aged HTPB binder material. Each 2D slice (110 μm thick) is an *XY* plane through the material with the aged surfaces at the top and bottom of the individual slices. The field of view for each slice is 2.5 mm × 3.5 mm and has a voxel size of 78 μm × 55 μm. The gray voxels designate image regions removed during analysis based on the error from the T_2 fits. For additional details see the text.

The complete 3D ^{1}H NMR T_2 map or image (individual 2D slices) for the aged HTPB/IPDI binder is shown in Figure 4. In this T_2 map the effects of thermooxidative aging on the HTPB polyurethane binder are visible. Near the aging surface (top and bottom of each individual slice) there is a layer ($\sim$ 100−200 μm thick) for which the spin−spin relaxation time T_2 has significantly decreased (blue-green regions) while the T_2 values in the interior remain long (red-yellow regions). The short T_2 near the surface ($T_2 \sim$ 600−800 μs) results from a reduction in local polymer mobility and is consistent with the hardening of the surface due to surface oxidation. The range of observed T_2 values are consistent with the $T_2 = 734$ μs measured for bulk aged HTPB binder (see Supporting Information). It is well know that these HTPB binders are subject to diffusion-limited oxidation (DLO) effects at higher temperatures and that the dominant aging process is related to chemical cross-linking, presumably due to free radical reactions involving the high concentration of unsaturation in the polymer.[3]

It has been forwarded that these apparent changes in T_2 relaxation times at the surfaces of the aged sample occur due to MRI-contrast resulting from other sources, including B_1 inhomogeneity or susceptibility effects, and not true T_2 relaxation. There are several arguments against this suggestion including: (1) The short T_2 values are only observed on two of the six total surfaces of the sample, and these two surfaces correspond to the surfaces in direct contact with the oxidative atmosphere. Susceptibility induced effects would be similar for all six surfaces. (2) The short T_2 values measured agree well with the T_2 value obtained from bulk aged HTPB binder (Supporting Information). (3) Shrinkage effects would impact the total ^{1}H density observed for voxels at the surface but should have minimal impact on the T_2 maps. (4) Likewise, B_1 heterogeneity is not significant since a solenoid coil with a length-to-diameter ratio of greater than one was used, and the sample dimensions were about half the coil diameter. In this case B_1 homogeneity is expected to vary by no more than 10% across the sample. Consequently, if B_1 homogeneity was poor, significant slice-to-slice variations in the T_2 maps shown in Figure 4 would be predicted, but such behavior is not observed. (5) Finally, it is know from the micromodulus profiling results (see below) that the surfaces of the aged HTPB binder that show short T_2 values also reveal a dramatic increase in the modulus. For these reasons we argue that the contrast effects we observed at the edges of the images in Figure 4 do in fact occur from local changes in the ^{1}H NMR T_2 relaxation time of the binder.

This variation in the T_2 relaxation times as a function of distance from the aging surface can also be seen in Figure 5, in which the measured T_2 (blue dots) are projected onto the *Y* axis perpendicular to the aging surfaces. The black line in Figure 5 is the mean T_2 relaxation time as a function from the aged surface, averaged over all image voxels in that *XZ* plane. There is clearly a spatial variation in T_2 relaxation times

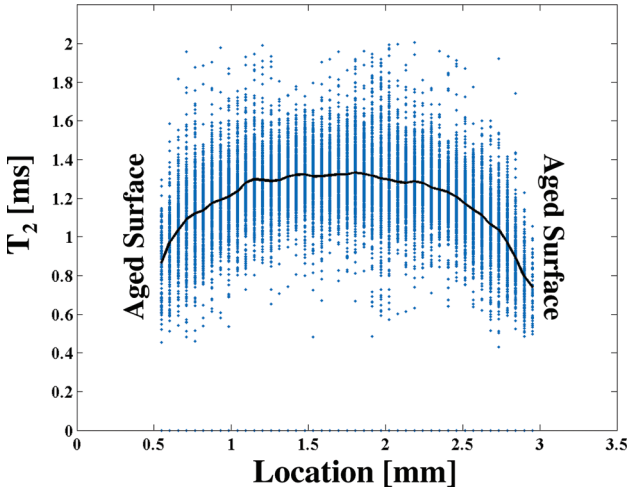

Figure 5. Plot of the 19 881 individually measured NMR T_2 values obtained from Figure 4 as a distance along the Y-axis perpendicular to the aging surfaces. The blue dots are the various T_2 values, and the black line is the mean T_2 across the material thickness.

across the HTPB binder, with the shortest T_2 relaxation time occurring at both aged surfaces. The range of average T_2 values are consistent with those obtained from bulk T_2 measurements (Supporting Information) which gave a $T_2 = 1.289$ ms for the unaged binder and $T_2 = 734$ μs for the aged binder. For this aged HTPB binder sample, the smooth variation in T_2 values across the entire sample dimension shows that there are physical changes occurring to the polymer dynamics in regions within ~1 mm from each of the aging surfaces, and at the center of the sample the aging effects are minimal (as compared to bulk unaged binder). The depth of this physical variation in properties appears more dramatic than the changes observed in previously reported micromodulus results.[3] This suggests that NMR T_2 mapping may be more sensitive to different changes in the local chain dynamics than can be detected in modulus measurements. Figure 5 also reveals a large distribution of T_2 relaxation times at a given spatial position, resulting from polymer heterogeneity not directly related to the propagating aging front. Further discussion into T_2 distributions is presented later.

One issue that needs to be discussed is the magnitude of error associated with the production of ^{1}H NMR T_2 relaxation maps. This analysis is required to determine whether the variations within the T_2 maps are the result of polymer heterogeneities or are the result of experimental error. In the present study imaging distortions such as Gibbs ringing or rf interference do not introduce significant error into the T_2 maps. The main source of error arises from the calculation of the T_2 for individual voxels and needs to be estimated and minimized. First, the range of expected T_2 values were measured from bulk T_2 NMR measurements (see Supporting Information) and allowed the careful selection of interpulse Hahn-echo delays (τ) to maximize the accuracy of the T_2 imaging measurement. Second, the bulk NMR T_2 measurements also demonstrated that the relaxation decay is very well described by a single exponential for the delay times utilized in the imaging experiments and that eq 1 can be used to estimate the T_2 relaxation time. To handle the error associated with the generation of T_2 maps from a very limited set of τ spacings, the distribution in T_2 errors was used to identify voxels with unacceptable levels of noise. Using all 23 540 signal-containing voxels measured for this 3D NMR image, a standard deviation σ in the T_2 fitting errors was obtained. Any image voxel with a fitting error greater than one σ deviation from the mean fitting error was assumed to be too noisy and was rejected. The rejected image voxels are rendered gray in all subsequent T_2 relaxation maps and were not utilized in subsequent analysis of the binder aging. When individual voxels are eliminated due to either no sample in that region (41 996 voxels) or voxels with unacceptable T_2 error (3659 voxels), there are still 19 881 individual T_2 measurements (voxels) that were used in the creation of the T_2 maps. This high number of individual T_2 measurements provides ample statistics in the analysis of variations in T_2. For example, in the calculation of the mean T_2 values as a function of position along Y shown in Figure 5, ~440 individual T_2 measurements were used to calculate each mean T_2 value. On the basis of the standard deviation of error in the T_2 fits, it was estimated that the error in the individual T_2 measurements was $\sim\pm0.1$ ms.

In previous NMR relaxation images of polymers, analysis of distributions of relaxation times and rates have been used to discuss heterogeneities in the physical properties of the polymer.[43,44,49,63] To explore similar effects in this aged HTPB binder sample, Figure 6 shows histogram plots of the measured T_2 values for four different regions of the sample. Figure 6a is the T_2 distribution from a surface layer 109 μm deep (2 voxels along Y) parallel to the aged (XZ) surface, averaged over a 548 μm section (5 slices along Z) near the top of the sample (refer to Figure 2c for definition of axes). Figure 6b is the T_2 distribution for the equivalent aged surface but represents an average over a 548 μm section (5 slices along Z) near the bottom of the sample. In a similar manner, parts c and d of Figure 6 are the T_2 distributions for an interior slice along the X-axis that was a 273 μm layer (5 voxels along Y) averaged over a 548 μm section (5 slices along Z) near the top and bottom of the binder sample, respectively. The dashed lines in Figure 6 designate the mean T_2 relaxation time for each histogram: (a) 0.83, (b) 0.86, (c) 1.34, and (d) 1.24 ms. The interior slices show a average T_2 (1.34 and 1.24 ms) that is longer than the T_2 observed near the aged surface (0.83 and 0.86 ms). This is also consistent with the variation in the mean T_2 plotted in Figure 5.

The histograms in Figure 6 reveal that the width of the T_2 distributions is much larger than the estimated error (±0.1 ms) for an individual T_2 measurement. This result demonstrates that the T_2 relaxation times, and correspondingly the local polymer dynamics and residual dipolar coupling, are spatially heterogeneous throughout the polymer. This heterogeneity is observed even with the relatively large volume element of 0.00 047 mm^3, which is the voxel size of the NMRI experiment, suggesting that polymer properties should be discussed on similar dimensions. Heterogeneities have previously been observed in NMRI studies of curing in natural rubbers and polybutadiene blends and were contributed to poor dispersion of accelerator and sulfur, along with differences in the solubility and diffusion of curing species.[66]

The changes in the T_2 distribution widths between the aged surfaces (Figure 6a,b) vs the interior portions (Figure 6c,d) are not drastically different, demonstrating

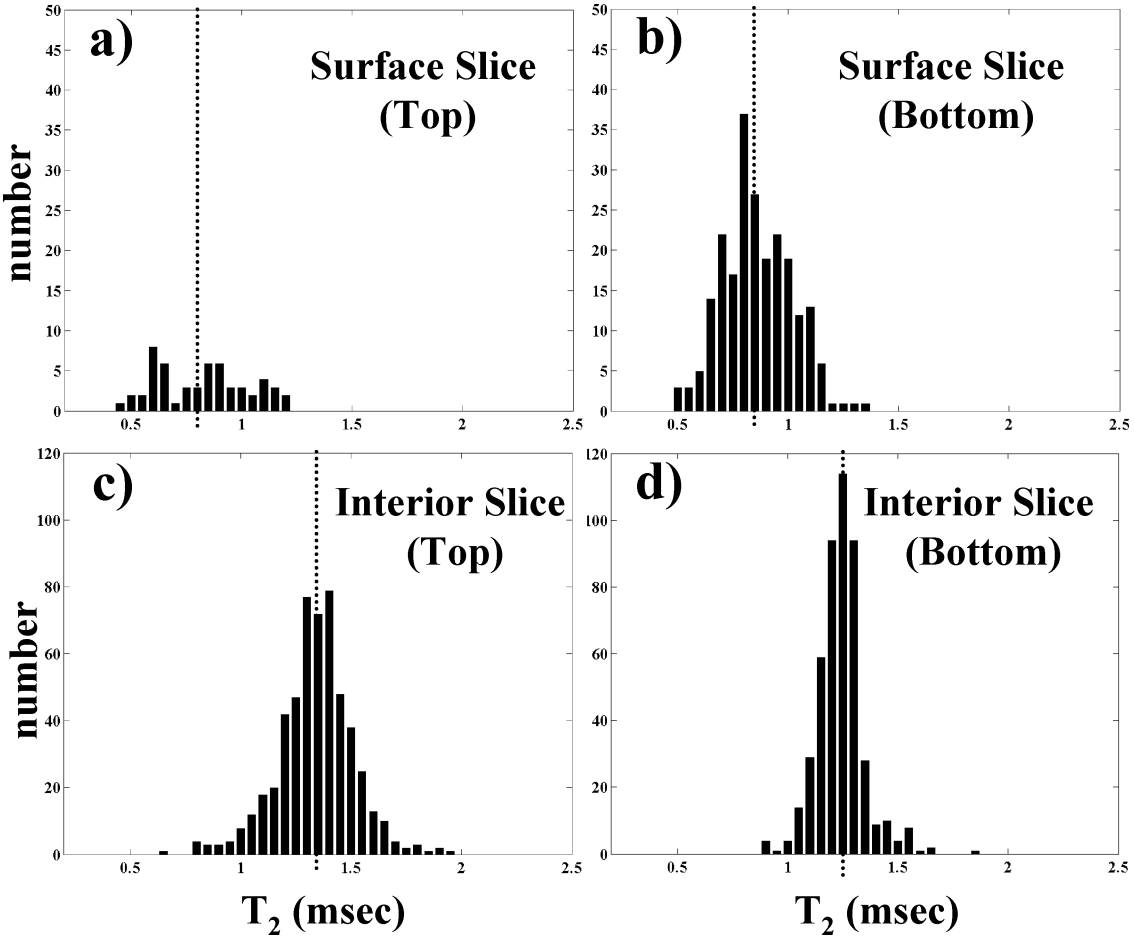

Figure 6. Histogram plots of the T_2 relaxation times measured for the thermooxidatively aged HTPB binder for a region representing the aged surface from (a) the top of the sample and (b) the bottom of the sample or an interior region from the (c) top of the sample and (d) bottom of the sample. Additional details are given in the text.

that in the case of the HTPB/IPDI binder thermooxidation does not dramatically increase the T_2 distributions as seen in other aging studies. There are also differences in the T_2 distributions arising whether the analysis was performed at the top or bottom of the aged polymer (Figure 6, a vs b and c vs d), revealing a variation in heterogeneity between the top and bottom of this binder sample (orthogonal to the aging surface) that is not directly related to the surface oxidation effects. This variation between top and bottom of the sample may have arisen due to initial variations in the HTPB binder prior to aging or more likely from long-distance aging effects related to the relative position within the large binder pad (2 cm × 2 cm × 3.5 mm) that this small imaging sample was cut. These spatial variations within the HTPB binder are presently being investigated.

Given the large T_2 distributions shown in Figure 6, some comment should be made about the ability to image minor aging effects within polymer samples. In the present investigation, the aged sample represents a heavily thermooxidized HTPB binder (8 days at 125 °C). Even with this high degree of aging, the mean T_2 only varies between ~0.8 and 1.3 ms (Figure 5), with an estimated error of about ±0.1 ms. The large T_2 distributions arising from spatial heterogeneities will therefore complicate distinguishing T_2 variations that are less than ~10%, making imaging studies of minor aging changes difficult. It has been shown that in some situations other NMR relaxation parameters ($T_{1\rho}$ or T_1) or the use of swelling solvents may provide a larger measure of changes in local polymer properties[5] and could be utilized to enhance NMR imaging studies of polymer aging.

It is known that correlations between NMR relaxation parameters and other measured physical properties can be developed.[67−69] It has been proposed that the spin−spin relaxation rate ($1/T_2$) should be linearly related to the modulus.[68] Figure 7a shows the previously reported micro elastic indentation modulus data perpendicular (along Y) to the aged surface obtained for the aged HTPB/IPDI binder.[3] The extreme hardening at the aged surfaces is readily apparent, with the measured elastic indentation modulus (E) increasing from 1.45 MPa in the interior to almost 20 MPa near the aged surface. It is known from unaged samples that the binder is a relatively soft material ($E \approx 0.7$ MPa). These data allow the correlation between the NMR measured spin−spin relaxation rate ($1/T_2$) and the modulus to be obtained and are shown in Figure 7b. Three distinct correlation regions are observed; at low modulus values $1/T_2$ is linear with E but shows two regions with different slopes. Region I shows a 0.164 ms^{-1} MPa^{-1} relationship, while region II has a 0.044 ms^{-1} MPa^{-1} relationship. Finally, near the surface where the modulus is greater than 10 MPa (region III) the linearity between $1/T_2$ and E is no longer observed. Care should be taken in the interpretation of region III because of the small number of modulus data points defining a very large change in modulus (Figure 7a) and the uncertainty of correlating

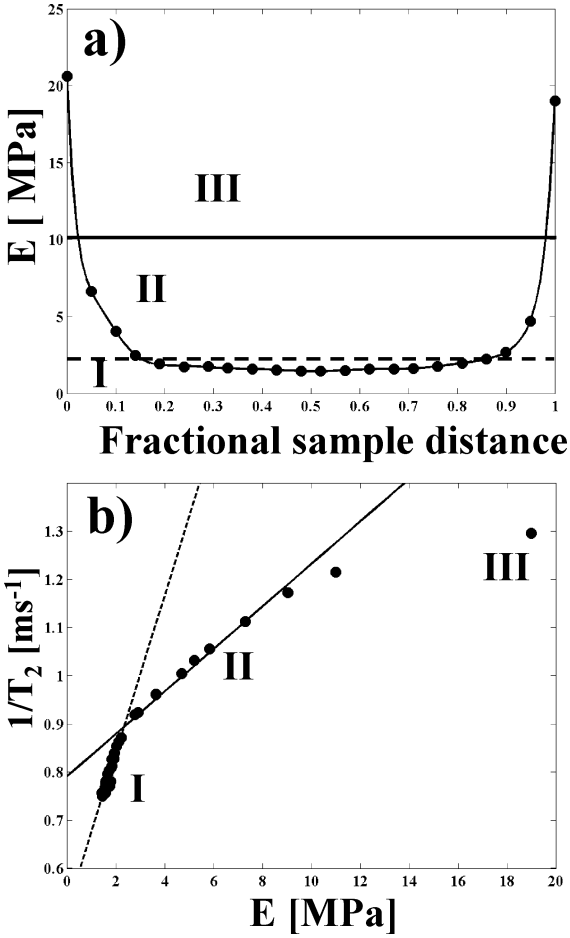

Figure 7. (a) Elastic indentation modulus (E) profile for the thermooxidatively aged HTPB binder, adapted from Celina et al. with permission.[3] The solid and dashed lines define the linear regions I and II. (b) Plot of the correlation between the mean ^{1}H NMR relaxation rate ($1/T_2$) obtained in Figure 5 and the elastic indentation modulus (E) in the aged HTPB binder. The dashed line indicates the linear fit to region I, while the solid line represents the linear fit to region II.

the exact sample edge between the R-NMRI and the modulus data.

The linearity observed between $1/T_2$ and E in regions I and II agrees well with predictions, but the appearance of the two different correlation regions was unexpected. Within each region the effect of cross-linking on the correlation time of the inherent polymer motions is similar, giving rise to the linear response. The change in slope between regions I and II (at $\sim$350 μm) indicates a dramatic variation in the respective molecular correlation times as a function of cross-link density. The interface between regions I and II may correlate to significant chemical changes that have occurred near the surface due to DLO effects. It is also clear that there are changes in the T_2 and E within the interior of the material (region I) where O_2 is not readily assessable, suggesting that the some of the T_2 changes are not directly DLO related.

Conclusion

In this work 3D ^{1}H NMR images and the corresponding ^{1}H spin−spin T_2 relaxation parameter maps were obtained for a thermooxidatively aged HTPB/IPDI polymer binder. While the spin density images did not show any clear indication of aging, the T_2 parameter maps clearly revealed heterogeneity due to aging within the sample. The majority of this heterogeneity resulted from diffusion-limited oxidation effects at the polymer surface, with the aged surfaces showing the most dramatic reduction in T_2 and correlation with an increase in the local elastic indentation modulus. In addition, dynamical heterogeneities throughout the polymer sample not related to aging effects were also observed but were not as dramatic as those seen for the aged surfaces. This investigation demonstrates that 3D NMR imaging can be used to probe the spatial variation of aging in polymer samples.

Acknowledgment. Sandia is a multiprogram laboratory operated by Sandia Corp., a Lockheed Martin Co., for the United States Department of Energy's National Nuclear Security Administration under Contract DE-AC04-94AL85000. This work was supported under the Sandia Research Foundation program. The imaging was performed at the William R. Wiley Environmental Molecular Sciences Laboratory (EMSL), a national scientific user facility sponsored by the Department of Energy's Office of Biological and Environmental Research and located at Pacific Northwest National Laboratory. The authors are also indebted to Sarah McIntyre for assistant in data analysis.

Supporting Information Available: ^{1}H NMR spin-echo T_2 decay curves obtained from the bulk unaged (Figure 1S) and aged (Figure 2S) HTPB/IPDI binders. This material is available free of charge via the Internet at http://pubs.acs.org.

References and Notes

(1) Celina, M.; Minier, L. M.; Assink, R. A. *CPIA Publ.* **2000**, *697*, 471.
(2) Celina, M.; Minier, L. M.; Assink, R. A. *Thermochim. Acta* **2000**, *384*, 343.
(3) Celina, M.; Graham, A. C.; Gillen, K. T.; Assink, R. A.; Minier, L. M. *Rubber Chem. Technol.* **2000**, *73*, 678.
(4) Assink, R. A.; Lang, D. P.; Celina, M. *J. Appl. Polym. Sci.* **2001**, *81*, 453.
(5) Assink, R. A.; Celina, M.; Gillen, K. T. *Polym. News* **2003**, *28*, 102.
(6) Assink, R. A.; Celina, M.; Minier, L. M. *J. Appl. Polym. Sci.* **2002**, *86*, 3636.
(7) Mowery, D. M.; Assink, R. A.; Celina, M. *Polymer* **2005**, *46*, 10919.
(8) George, G.; Celina, M. In *Handbook of Polymer Degradation*; Hamid, S. H., Ed.; Marcel Dekker: New York, 2000; p 277.
(9) Celina, M.; George, G. A. *Polym. Degrad. Stab.* **1993**, *40*, 323.
(10) Celina, M.; George, G.; Billingham, N. C. In *Polymer Durability: Degradation, Stabilization, and Lifetime Prediction*; Clough, R. L., Billingham, N. C., Gillen, K. T., Eds.; American Chemical Society: Washington, DC, 1996; p 159.
(11) Billingham, N. C. In *Oxidative Inhibition in Organic Materials*; Pospisil, J., LKlemchuk, P. P., Eds.; CRC Press: Boca Raton, FL, 1990; p 249.
(12) Gillen, K. T.; Clough, R. L. *Polymer* **1992**, *33*, 4358.
(13) Wise, J.; Gillen, K. T.; Clough, R. L. *Polymer* **1997**, *38*, 1929.
(14) Gillen, K. T.; Terrill, E. R.; Winter, R. *Rubber Chem. Technol.* **2001**, *74*, 428.
(15) Blümich, B.; Blümler, P.; Gasper, L.; Guthausen, A.; Göbbels, V.; Laukemper-Ostendorf, S.; Unseld, K.; Zimmer, G. *Macromol. Symp.* **1999**, *141*, 83.
(16) Callaghan, P. T. *Principles of Nuclear Magnetic Resonance Microscopy*; Claredon Press: Oxford, 1991.
(17) Chang, C.; Komoroski, R. A. *Macromolecules* **1989**, *22*, 600.
(18) Sarkar, S. N.; Komoroski, R. A. *Macromolecules* **1992**, *25*, 1420.
(19) Blümler, P.; Blümich, B. *Macromolecules* **1991**, *24*, 2183.
(20) Kuhn, W.; Barth, P.; Hafner, S.; Simon, G.; Schneider, H. *Macromolecules* **1994**, *27*, 5773.
(21) Blümich, B. *NMR Imaging of Materials*; Oxford Science Publications: Oxford, 2000; Vol. 57.
(22) Götz, J.; Eisenreich, N.; Geissler, A.; Geissler, E. *Propellant, Explos., Pyrotech.* **2002**, *27*, 179.
(23) Smith, S. R.; Koenig, J. L. *Macromolecules* **1991**, *24*, 3496.

(24) Rana, M. A.; Koenig, J. L. *Macromolecules* **1994**, *27*, 3727.
(25) Lauenstein, Å.; Tegenfeldt, J.; Kuhn, W. *Macromolecules* **1998**, *31*, 3886.
(26) Adriaensens, P.; Pollaris, A.; Vanderzande, D.; Gelan, J.; White, J. L.; Kelchtermans, M. *Macromolecules* **2000**, *33*, 7116.
(27) Braun, J.; Klein, M. O.; Bernarding, J.; Leitner, M. B.; Mika, H. D. *Polym. Testing* **2003**, *22*, 761.
(28) Lees, T. J.; Balcom, B. J. *Magn. Reson. Chem.* **2003**, *41*, 229.
(29) Malak, M.; Hill, D. J. T.; Whittaker, A. K. *Polym. Int.* **2003**, *52*, 1740.
(30) Adriaensens, P.; Pollaris, A.; Rulkens, R.; Litvinov, V. M.; Gelan, J. *Polymer* **2004**, *45*, 2465.
(31) Kusmia, S.; Kozak, M.; Szczesniak, E.; Domka, L.; Jurga, S. *Solid State Nucl. Magn. Reson.* **2004**, *25*, 173.
(32) Baumgarter, S.; Lahajnar, G.; Sepe, A.; Kristl, J. *Eur. J. Pharm. Biopharm.* **2005**, *59*, 299.
(33) Adriaensens, P.; Pollaris, A.; Kelchtermans, M.; Gelan, J. *Macromolecules* **2003**, *36*, 706.
(34) Gussoni, M.; Greco, F.; Mapelli, M.; Vezzoli, A.; Ranucci, E.; Ferruti, P.; Zetta, L. *Macromolecules* **2002**, *35*, 1722.
(35) Emid, S.; Creyghton, J. H. N. *Physica* **1985**, *128B*, 81.
(36) Balcom, B. J.; MacGregor, R. P.; Beyea, S. D.; Green, D. P.; Armstrong, R. L.; Bremner, T. W. *J. Magn. Reson. A* **1996**, *123*, 131.
(37) Beyea, S. D.; Balcom, B. J.; Mastikhin, I. V.; Bremner, T. W.; Armstrong, R. L.; Grattan-Bellow, P. E. *J. Magn. Reson.* **2000**, *144*, 255.
(38) Szomolanyi, P.; Goodyear, D.; Balcom, B. J.; Matheson, D. *Magn. Reson. Imag.* **2001**, *19*, 423.
(39) Fang, Z.; Hoepfel, D.; Winter, K. *Magn. Reson. Imag.* **2001**, *19*, 501.
(40) Chudek, J. A.; Hunter, G. *Annu. Rep. NMR Spectrosc.* **2002**, *45*, 151.
(41) Ghosh, P.; Laidlaw, D. H.; Fleischer, K. W.; Barr, A. H.; Jacobs, R. E. *IEEE Trans. Med. Imag.* **1995**, *14*, 616.
(42) Barth, P.; Hafner, S.; Denner, P. *Macromolecules* **1996**, *29*, 1655.
(43) Barth, P.; Hafner, S. *Magn. Reson. Imag.* **1997**, *15*, 107.
(44) Chaumette, H.; Grandclaude, D.; Canet, D. *J. Magn. Reson.* **2003**, *163*, 369.
(45) Traub, B.; Hafner, S.; Wiesner, U.; Spiess, H. W. *Macromolecules* **1998**, *31*, 8585.
(46) Prado, P. J.; Gasper, L.; Fink, G.; Blümich, B. *Appl. Magn. Reson.* **2000**, *18*, 177.
(47) Schneider, M.; Demco, D. E.; Blümich, B. *Macromolecules* **2001**, *34*, 4019.
(48) Canet, D.; Malveau, C.; Grandclaude, D.; Tekely, P.; Beaume, F.; Germain, Y. *Macromol. Symp.* **2005**, *220*, 33.
(49) Malveau, C.; Grandclaude, D.; Canet, D. *J. Magn. Reson.* **2001**, *150*, 214.
(50) Blümich, B. *Concepts Magn. Reson.* **1999**, *11*, 147.
(51) Blümich, B. *Concepts Magn. Reson.* **1998**, *10*, 19.
(52) Blümich, B. *Concepts Magn. Reson.* **1999**, *11*, 71.
(53) Schneider, M.; Demco, D. E.; Blümich, B. *J. Magn. Reson.* **1999**, *140*, 432.
(54) Sotta, P.; Fülber, C.; Demco, D. E.; Blümich, B.; Spiess, H. W. *Macromolecules* **1996**, *29*, 6222.
(55) Callaghan, P. T.; Samulski, E. T. *Macromolecules* **1997**, *30*, 113.
(56) Maxwell, R. S.; Balazs, B. *Nucl. Instrum. Methods Phys. Res. B* **2003**, *208*, 199.
(57) Gee, R. H.; Maxwell, R. S.; Balazs, B. *Polymer* **2004**, *45*, 3885.
(58) Fechete, R.; Demco, D. E.; Blümich, B. *J. Magn. Reson.* **2003**, *165*, 9.
(59) Garbarczyk, M.; Kuhn, W.; Klinowski, J.; Jurga, S. *Polymer* **2002**, *43*, 3169.
(60) Spyros, A.; Kimmich, R.; Briese, B. H.; Jendrossek, D. *Macromolecules* **1997**, *30*, 8218.
(61) Chudek, J. A.; Hunter, G. *J. Mater. Sci., Lett.* **1992**, *11*, 222.
(62) Hafner, S.; Barth, P. *Magn. Reson. Imag.* **1995**, *13*, 739.
(63) Cherry, B. R.; Alam, T. M. *Polymer* **2004**, *45*, 5611.
(64) Low, D. A.; Dempsey, J. F.; Ventatesan, R.; Mutic, S.; Markman, J.; Haacke, E. M.; Purdy, J. A. *Med. Phys.* **1999**, *26*, 1542.
(65) Beyea, S. D.; Balcom, B. J.; Prado, P. J.; Cross, A. R.; Kennedy, C. B.; Armstrong, R. L.; Bremner, T. W. *J. Magn. Reson.* **1998**, *135*, 156.
(66) Klei, B.; Koenig, J. L. *Acta Polym.* **1997**, *48*, 199.
(67) Cohen-Addad, J. P.; Labouriau, A. *J. Chem. Phys.* **1990**, *93*, 2911.
(68) Cohen-Addad, J. P.; Phan Thanh, B.; Montes, H. *Macromolecules* **1997**, *30*, 4374.
(69) Maxwell, R. S.; Cohenour, R.; Sung, W.; Solyom, D.; Patel, M. *Polym. Degrad. Stab.* **2003**, *80*, 443.

MA051906Y